ADVANCED MATERIALS INTERFACES
Open Access
www.advmatinterfaces.de

Intrinsically Cross-Linked ECM-Like Multilayers for BMP-2 Delivery Promote Osteogenic Differentiation of Cells

*Reema Anouz, Tamaradobra Selekere, Adrian Hautmann, Catharina Husteden, Matthias Menzel, Christian Woelk, Christian E. H. Schmelzer, and Thomas Groth**

Dedicated to the pure soul of my little brother who passed away in 2021 during the Corona pandemic

Surface coatings prepared by layer-by-layer technique permit loading of growth factors (GFs) and their spatially controlled release. Here, native chondroitin sulfate (nCS), oxidized CS (oCS100), or mixture of both (oCS50) are combined with collagen I (Col I) to fabricate polyelectrolyte multilayers (PEMs) that exhibit structural, mechanical, and biochemical cues like the natural extracellular-matrix. The use of oCS enables intrinsic cross-linking of PEM that offers higher stability, stiffness, and better control of bone morphogenetic protein-2 (BMP-2) release compared to nCS. oCS100 PEMs have enhanced stiffness, promote Col I fibrillization, and present BMP-2 in a matrix-bound manner. oCS50 PEMs show intermediate effects on osteogenesis, soft surface, high water content but also moderately slow BMP-2 release profile. C2C12 myoblasts used for osteogenesis studies show that oCS PEMs are more stable and superior to nCS PEMs in supporting cell adhesion and spreading as well as in presenting BMP-2 to the cells. oCS PEMs are triggering more osteogenesis as proved by the quantitative real-time polymerase chain reaction, immune and histochemical staining. These findings show that intrinsic cross-linking in oCS/Col I multilayers provides a successful tool to control GFs delivery and subsequent cell differentiation which opens new opportunities in regenerative therapies of bone and other tissues.

1. Introduction

Unlike the usual nature of bone tissue, which is capable to regenerate by itself, large bone defects are one of the most faced challenges in orthopedic surgeries. Such defects, which occur after fractures or tumor resections, do not heal on their own and often require surgical intervention.[1] Since the gold standard method using bone autografts or allografts to regenerate bone still has its drawbacks and limitations, tissue engineering has emerged as an alternative approach.[2] Further, biomaterials used for tissue engineering approaches are mostly of synthetic origin.[3] Therefore, lacking biochemical cues that are usually present in the extracellular matrix (ECM). In native tissues, cells reside in the ECM which is a microenvironment filling the space among cells and varies from one tissue type to another providing each tissue with unique characteristics and plays many important key roles in cell adhesion, migration, proliferation, and differentiation through presentation of crucial biochemical and biomechanical cues.[4] Glycosaminoglycans (GAGs) and fibrous proteins (e.g., collagen I) are major components of the ECM.[5] Collagen I (Col I) does not only provide topographical cues and mechanical strength for tissues but also exhibits many biological functions such as mediating cell attachment and spreading.[6] GAGs such as chondroitin sulfate

R. Anouz, T. Selekere, A. Hautmann, T. Groth
Department of Biomedical Materials
Institute of Pharmacy
Martin Luther University Halle-Wittenberg
Heinrich-Damerow-Strasse 4, 06120 Halle Saale, Germany
E-mail: thomas.groth@pharmazie.uni-halle.de

The ORCID identification number(s) for the author(s) of this article can be found under https://doi.org/10.1002/admi.202201596.

DOI: 10.1002/admi.202201596

C. Husteden
Biochemical Pharmacy
Institute of Pharmacy
Martin Luther University Halle-Wittenberg
Wolfgang-Langenbeck-Straße 4, 06120 Halle Saale, Germany

M. Menzel, C. E. H. Schmelzer
Fraunhofer Institute for Microstructure of Materials and Systems IMWS
Walter-Hülse-Straße 1, 06120 Halle Saale, Germany

C. Woelk
Pharmaceutical Technology
Medical Faculty
University Leipzig
Eilenburger Straße 15a, 31, 04317 Leipzig, Germany

T. Groth
Interdisciplinary Center of Material Research and Interdisciplinary Center of Applied Research
Martin Luther University Halle-Wittenberg, Halle
06099 Saale, Germany

(CS) and hyaluronic acid (HA) play many important roles in cell growth and differentiation when interacting with cytokines, proteins, and cell receptors.[7] Hence, the ECM plays a role as a reservoir for storage and release of growth factors (GFs) such as bone morphogenetic protein-2 (BMP-2),[1,8] which induces the differentiation of mesenchymal stem cells (MSCs) and nonosteogenic cell lines such as C2C12 myoblasts into osteoblasts.[9] Therefore, scaffolds and biomaterials that mimic the ECM constitute a very promising strategy to induce tissue regeneration due to the unique properties of the ECM. Efforts to tailor the biocompatibility and to introduce biochemical cues to synthetic biomaterials have been made through physical, chemical, and biological surface modification techniques that were employed to modify biomaterials' surfaces due to their importance in creating the very first response when implanted in the body.[10] Layer-by-layer (LbL) is a physical modification technique that relies on alternative adsorption of oppositely charged polyelectrolytes to produce thin polyelectrolytes multilayers (PEMs)[11] that vary in their thickness, surface charge, wettability, viscoelasticity, and topography by varying the assembly conditions, medium characteristics, and the polyelectrolytes used.[12,13] In bone repair field, metals, ceramics, and polymers are used as implant materials. Since, multilayers can be deposited by LbL on any kind of substrate, it is an attractive surface modification technique for implantable devices; particularly when bioactive coatings mimicking composition of bone matrix and delivery of bioactive molecules are desired.[14] Due to its versatility, simplicity, low cost, and the use of water as a solvent, LbL enables the insertion of sensitive biomolecules like proteins and GFs and release them in a sustained manner over-time while preserving their bioactivity.[13] Using ECM biomolecules as polyelectrolytes in LbL is one of the strategies used to mimic the ECM properties for tissue regeneration. In that regard, GAGs and Col I are suitable candidates representing polyanion and polycation, respectively, which permits their use as building blocks for PEMs to create a biomimetic environment offering specific interactions with cell receptors and GFs.[10] Moreover, chemical cross-linking has been widely used to improve the stability of multilayers.[15–17] However, it causes changes in the physiochemical properties of the multilayers[18] and leads to cytotoxicity.[19] In a previous work, it was found that functionalization of GAGs with aldehyde groups through oxidation allows their immobilization on amino functionalized surface at which the bioactivity of the oxidized GAGs was not altered.[20] This functionalization method made the oxidized GAGs useful candidates to be used for generation of bioactive surface coatings. Further, Zhao et al. employed the latter functionalization method to fabricate multilayers with intrinsic cross-linking (covalent bond) between the aldehyde groups on the oxidized GAGs and the amino groups of Col I. An enhanced stability, Col I fibrillization, and cell adhesion were the characteristics of the intrinsically cross-linked multilayers compared to native GAGs multilayers.[21] Hence, we thought of using the same cross-linking method not only to enhance the multilayers properties but also to study it as a tool to control BMP-2 release and presentation to cells in order to achieve osteogenic differentiation of cells using multilayers exhibiting both physical and biochemical cues like the natural ECM. It is also worth mentioning that the cytotoxicity of this intrinsic cross-linking method of PEM using different cell types was already studied previously and revealed no toxic effect.[8,21,22] Thus, cytotoxicity measurements will not be performed again in this study.

Since Col I is a major protein in bone tissue[23] that has a significant impact on osteogenesis, it was used in this study as a polycation. Here, we studied multilayers composed of either oxidized chondroitin sulfate (oCS100), native chondroitin sulfate (nCS), or a 50:50 mixture of both (oCS50) together with Col I as polycation. The 50:50 mixture was introduced in this study to see the effect of the molecular composition on multilayers' characteristics and cellular behavior. The efficiency of the intrinsic cross-linking in controlling BMP-2 release and presentation was studied, in addition to physiochemical properties of the multilayers as well as the biological studies using C2C12 cells. C2C12 cells were chosen due to their potency to differentiate into either myotubes or osteoblasts. They have been used previously by other groups for studying BMP-2 signaling because of the presence of BMP receptor on C2C12 cells.[24] Therefore, C2C12 cells are responsive to both soluble[9] and matrix-bound BMP-2[25] with alkaline phosphatase (ALP) and Osterix expression being measurable after 3 days, while MSCs need at least 1 week to have detectable expression.[26] Results show that oCS/Col I multilayers are superior in many aspects, particularly in controlling BMP-2 release, presentation, and osteogenic differentiation of C2C12, compared to nCS/Col I multilayers. **Figure 1** illustrates the various multilayers used in this study and the occurring molecular interactions.

2. Results

2.1. Characterization of PEMs Properties

2.1.1. Multilayers Formation and Thickness

The multilayers formation of the various systems was controlled in a real-time measurement via quartz crystal microbalance with dissipation monitoring (QCM-D) as shown in **Figure 2**A–D. In general, it was shown that the frequency was decreasing after each layer for all PEMs, indicating that mass is added during deposition. However, the oCS50 PEMs exhibited higher decrease in frequency compared to the nCS and oCS100 PEMs. A rapid decrease in frequency from the base line was observed after the adsorption of the cationic poly(ethylene imine) (PEI). This also corresponded to a rapid increase in the energy dissipation in the layer, as shown in Figure 2B. It was possible to obtain information about the viscoelastic properties of the PEMs in term of change in dissipation. The increase in the energy dissipated through the multilayers formation was the highest for oCS50 PEMs followed by oCS100 and the lowest energy dissipation was observed for nCS, indicating that oCS50 PEMs have the softest layers. The PEM thickness was calculated using two types of equations: Sauerbrey equation, which is usually used with rigid, evenly distributed layers, and the Voigt model, which takes into consideration the contribution of the viscoelasticity to the sensed mass.[27] The latter is most probably more reliable to calculate the thickness in our study, since the change in energy dissipation is quite high and the analyzed PEMs are assumed to be viscoelastic layers.

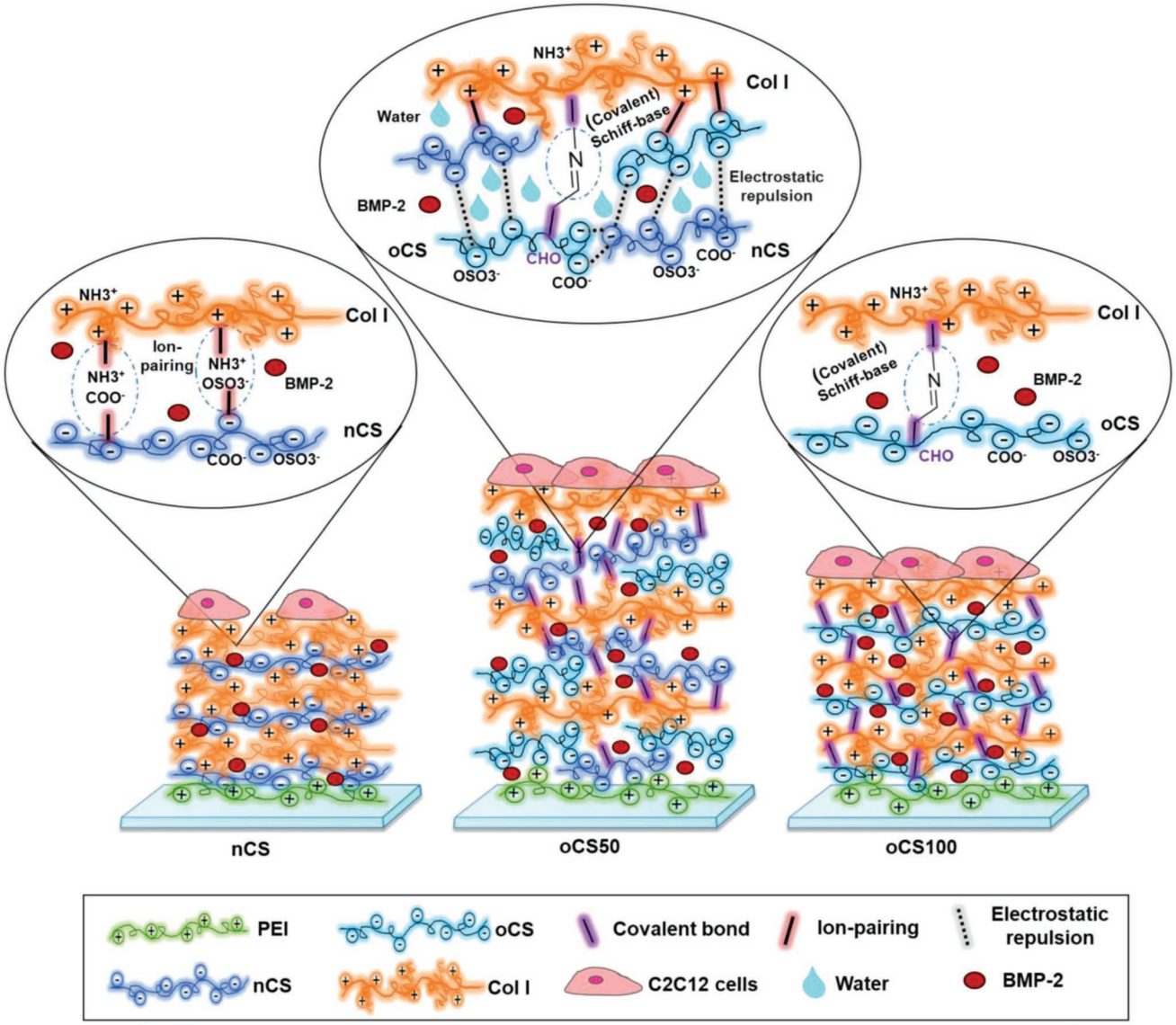

Figure 1. Illustration of the multilayers used in this study. Total of 17 layers. nCS is nCS/Col I multilayers, oCS50 is oCS50/Col I multilayers, and oCS100 is oCS100/Col I multilayers with oCS having oxidation degree of 2.77%. nCS depends mainly on ion pairing while oCS50 relies mainly on covalent binding and to a smaller extent on ion pairing, resulting in free negatively charged groups that lead to electrostatic repulsion, attraction of more water, and swelling. oCS100 is depending only on covalent binding.

The detected change in resonance frequency as a function of multilayers' build-up has been converted to the Sauerbrey adsorbed amount, as shown in Figure 2D. Further, by assuming that the density of the layer, viscosity of the bulk liquid, and fixed density layer are 1000 kg m^{-3}, 1 mPas, and 1400 kg m^{-3}, respectively,[27] it was possible to estimate the thickness as a function of the number of layers during the build-up of the PEMs as shown in Figure 2C. Value of ≈155, 140, and 128 nm for the final thickness was obtained for oCS50, oCS100, and nCS PEMs, respectively.

2.1.2. Wettability and Dry Thickness Measurements

As shown in **Figure 3**, all PEM systems showed moderate water contact angle (WCA) values around 50°, indicating that all PEMs are moderately hydrophilic compared to the plain glass (control) that showed WCA below 35°. Further, after measuring the dry thickness via ellipsometry, significantly thicker multilayers were obtained for oCS100 PEMs (≈32 nm) and oCS50 (≈31 nm) in comparison to nCS PEMs (≈24 nm).

2.1.3. Topography, Stiffness, and Roughness of PEMs

The surface topography, stiffness, and roughness of clean Si wafers and all PEMs were analyzed by atomic force microscopy (AFM) in wet state and under ambient laboratory conditions. **Figure 4**A shows that the topography of final layers of all PEM systems was characterized by the presence of Col I fibers. The fibrillization of Col I was supported on all BMP-2

ADVANCED MATERIALS INTERFACES
Open Access
www.advmatinterfaces.de

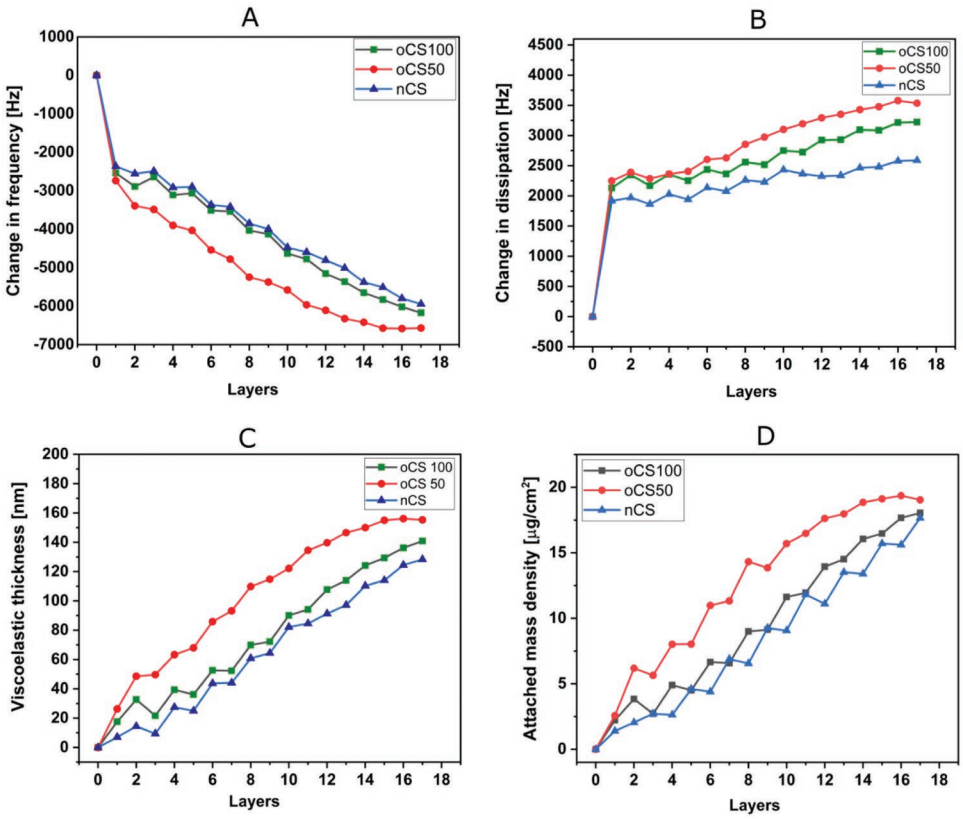

Figure 2. Film growth monitored in situ by QCM-D for oCS100, oCS50, and nCS multilayers. PEMs of oxidized chondroitin sulfate (oCS100), native chondroitin sulfate (nCS), or a mixture of both (oCS50) were prepared with Col I as polycation. A) Change in frequency shifts. B) Change in dissipation. C) Representation of viscoelastic thickness calculated in (nm) using voigt-based model. D) Representation of the attached mass calculated using Sauerbrey equation. The 1st layer is PEI, even numbers refer to native or oxidized CS and odd numbers refer to Col I. $n = 2$.

nonloaded multilayers with slight differences. oCS100 and oCS50 PEMs had significantly thicker Col I fibers than nCS PEMs (Figure 4B). On nonloaded samples (*BMP-2-*), oCS100 PEMs were showing the highest stiffness and roughness while oCS50 PEMs had the softest surface. A noticeable decrease in Col I fibers' thickness was observed after BMP-2 loading on all BMP-2-loaded PEMs. This decrease was reflected in a decrease in Young's modulus as well. However, oCS100 and oCS50 PEMs were more resistant and stable than nCS PEMs which were prone to complete loss of Col I fibers after BMP-2 loading. This Col I loss on nCS PEMs could have led to some rearrangement making the silicone substrate more prominent, which was reflected in a false positive increase in Young's modulus of nCS PEMs (Figure 4C). Further, the roughness of nonloaded PEMs was the highest for oCS100 PEMs, lesser for oCS50, and the least for nCS PEMs. The dissolution of Col I fibers

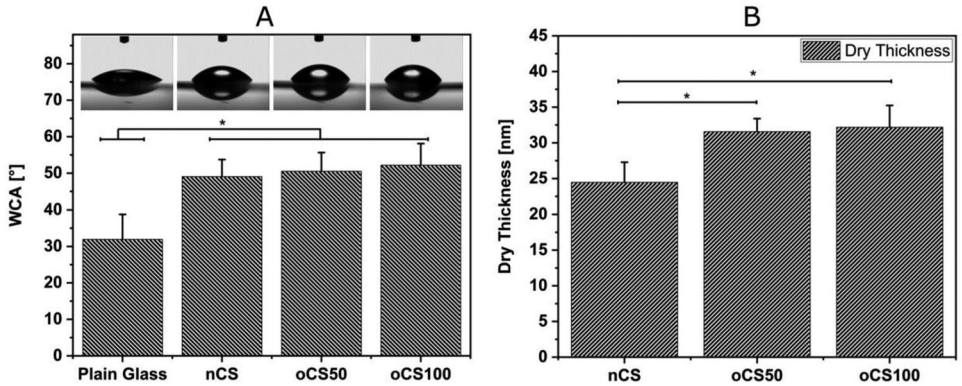

Figure 3. A) Static WCA measurements after multilayers formation up to 17 layers. Multilayers of oxidized chondroitin sulfate (oCS100), native chondroitin sulfate (nCS), or a mixture of both (oCS50) were prepared with Col I as polycation. Results are presented as means ± SD of four measurements taken from each sample for each multilayers system. B) Measurements of dry thickness taken by ellipsometry after formation of 17 layers of the various multilayers. Results represent means ± SD. $n = 4$. (*) data are significantly different.

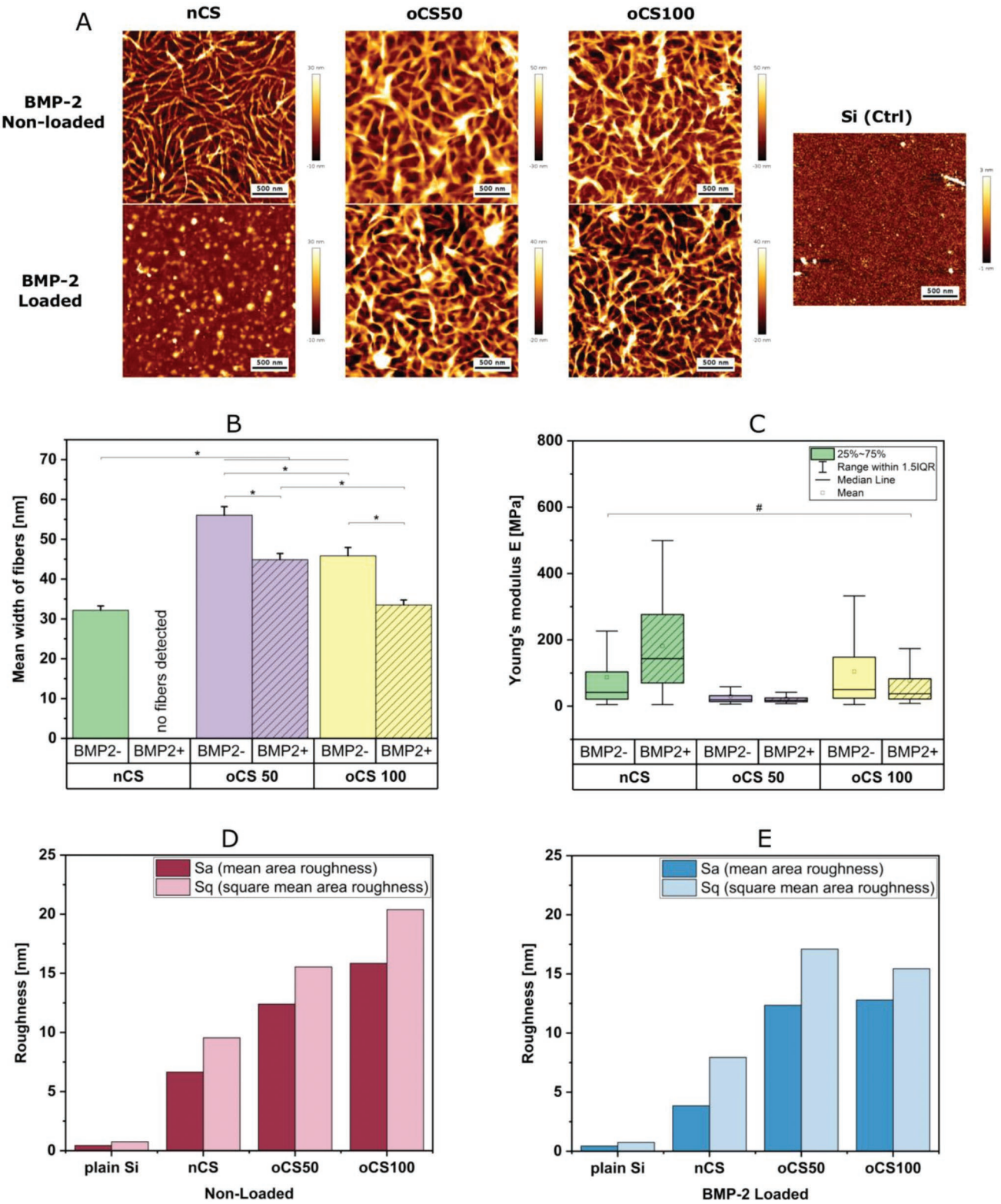

Figure 4. A) Surface topography of type I collagen (Col I) terminated multilayers (17th layer) visualized by atomic force microscopy (AFM). Multilayers of oxidized chondroitin sulfate (oCS100), native chondroitin sulfate (nCS), or a mixture of both (oCS50) were prepared with Col I as polycation. (Scale bar: 500 nm.) (*) data are significantly different. B) Quantification of Col I fibers diameter on the various multilayers using *FSegment* program. The program traces all fibers and measures the width of each fiber every 5 pixel (equals 48.5 nm). All measuring points per sample were then cumulated and analyzed. *BMP+* refers to BMP-2 loaded multilayers and *BMP-* refers to BMP-2 nonloaded multilayers. C) Young's modulus (elasticity) measurements by AFM. The Young's modulus *E* for each pixel was determined. All data are significant to each other except # ($p \leq 0.05$ Kruskal–Wallis-ANOVA, Dunn post hoc, $n = 131.072$). D) Surface roughness measurements of BMP-2 nonloaded multilayers. E) Surface roughness measurements of BMP-2 loaded multilayers.

affected the surface roughness, hence, a decrease in roughness was observed after loading BMP-2 to all types of PEMs (Figure 4D,E).

2.2. BMP-2 Adsorption and Release Studies

From the confocal laser scanning microscopy (CLSM) images and the quantification of BMP-2 adsorbed by the multilayers' surfaces (**Figure 5**A,B), it was concluded that BMP-2 adsorbed the most on oCS100 PEMs followed by oCS50 while the least was on nCS PEMs. However, a significant decrease of adsorbed BMP-2 was noticed after 7 days of incubation in Dulbecco's modified Eagle's medium (DMEM) for all PEMs. Further, regarding BMP-2 release, all PEMs were releasing the loaded BMP-2 over time in a sustained release manner. However, oCS100 PEMs with intrinsic cross-linking were able to store and present the majority of the loaded BMP-2 to the cells in a matrix-bound manner through releasing the least amounts over time (47 ng mL^{-1} on day 7) compared to oCS50 and nCS PEMs;

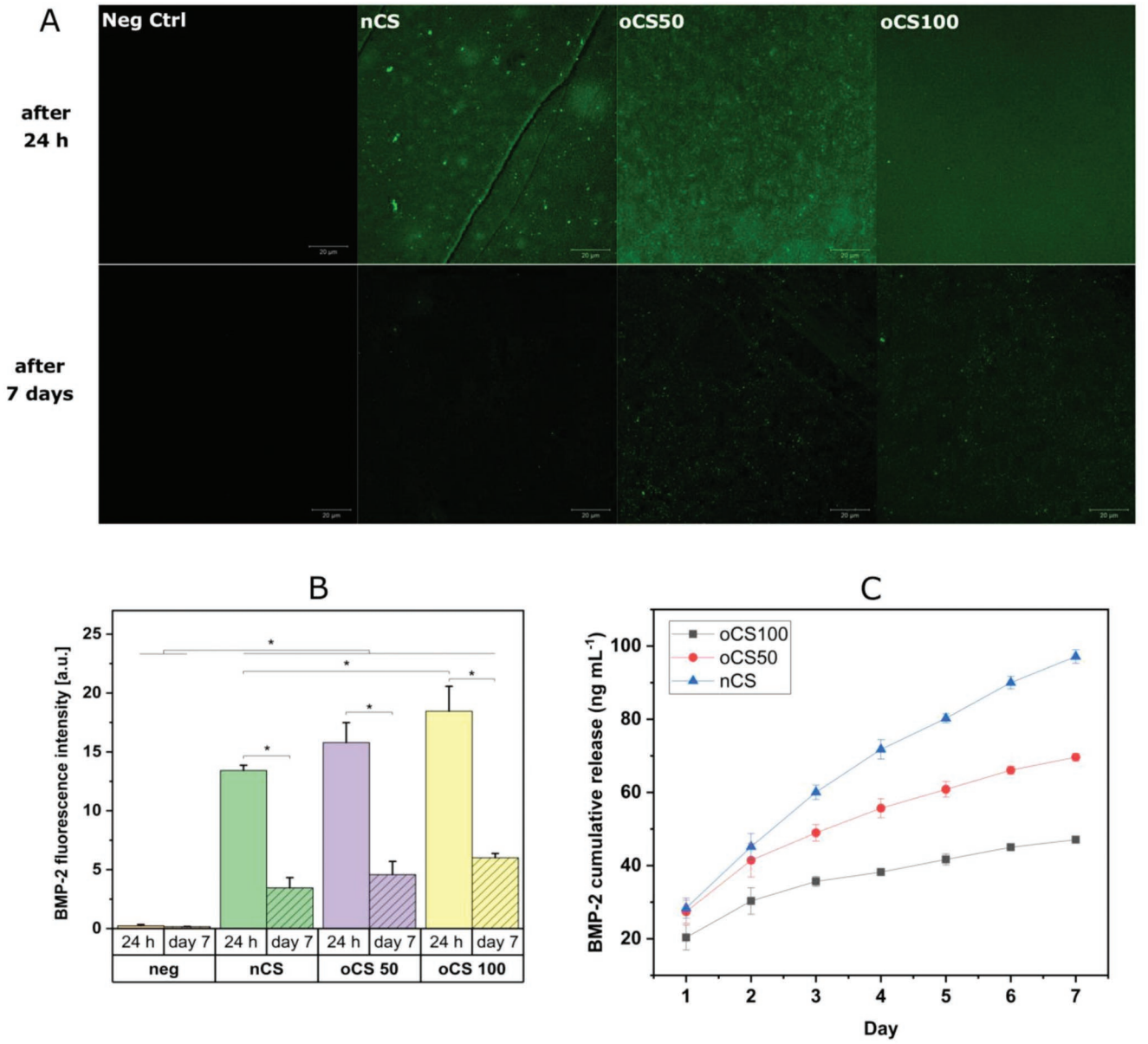

Figure 5. Multilayers of oxidized chondroitin sulfate (oCS100), native chondroitin sulfate (nCS), or a mixture of both (oCS50) were prepared with Col I as polycation. Neg Ctrl is plain glass and no BMP-2 was added. A) CLSM images of BMP-2 adsorbed at the various multilayers surfaces, after 24 h (the first row) and 7 days (the second row) of incubation in DMEM. (Scale bar: 20 µm.) B) Semiquantification of BMP-2 adsorbed on multilayers surface by quantifying the fluorescence intensity in CLSM images. The mean intensity was extracted by ImageJ 1.53c. (*) refers to significant difference, $p \leq 0.05$. C) Cumulative BMP-2 release from the various multilayers measured by ELISA over 7 days after loading BMP-2 (10 µg mL^{-1}) for overnight. Results are means ± SD. $n = 6$ replicates of each multilayers system.

as illustrated in Figure 5C. Released GFs have short life-time[28] while matrix-bound is the effective form of GFs presentation to cells, as shown in previous studies by the group of Picart.[29] Further, since the initial differentiation of C2C12 cells into functional osteoblasts is detectable during the first 3–7 days, characterized by upregulation of ALP,[26] BMP-2 release was only measured for 7 days. Despite that all PEMs were having a similar first release value (between 20 and 29 ng mL^{-1}), nCS PEMs, which lack intrinsic cross-linking and are mainly dependent on ion pairing, could not retain the loaded BMP-2 but rather released it much faster to the solution (97 ng mL^{-1} on day 7). However, oCS50 PEMs, partially depending on ion pairing and more on covalent binding, could balance this high release to a more moderate behavior (≈70 ng mL^{-1} on day 7). Moreover, after checking the BMP-2 release kinetics fitting from the multilayers, it was concluded that the BMP-2 release in this study fits to the Higuchi model (see the Supporting Information). This means that the release was diffusion dependent and was not relying on the degradation of the matrix or the multilayers.[30] Therefore, the type of binding inside the multilayers is mainly affecting and controlling the BMP-2 release and presentation.

2.3. BMP-2 Internalization Study

BMP-2 was internalized into the cells on all PEMs in general (**Figure 6**). However, more staining of BMP-2 molecules was observed on oCS PEMs than on nCS PEMs indicating more internalization on intrinsically cross-linked PEMs (oCS100, oCS50) due to the presentation of BMP-2 to cells in a matrix-bound manner. Further, lesser BMP-2 internalization was observed on pos Ctrl where BMP-2 is present to the cells in a soluble state and not as matrix-bound like in the oCS PEMs, indicating much slower internalization of soluble BMP-2. Similar results were for nCS PEMs which were offering most of the BMP-2 in a released (soluble) state. The neg Ctrl containing no BMP-2 showed no staining of BMP-2. On all PEMs, the internalization of BMP-2 in permeabilized cells after 24 h was clear in the form of dots (green) representing BMP-2 molecules.

2.4. C2C12 Cell Adhesion Study

To explore whether the loaded BMP-2 has any effect on cell adhesion, two sets of samples were used, original (nonloaded) and BMP-2-loaded multilayers, as shown in **Figure 7**. All original PEMs supported cell adhesion in general with small variances regarding the number of C2C12 cells (Figure 7A). However, on original PEMs (nonloaded), cell spreading was higher on intrinsically cross-linked PEMs (i.e., on oCS100 and oCS50 PEMs) than on nCS PEMs and pos Ctrl, characterized by more spread and elongated cells with significantly longer actin filaments (red) which could be seen from the CLSM images as well as from the quantification of cell area and actin filaments length per cell. Nevertheless, no organization of vinculin molecules (green) in focal adhesions (FAs) could be detected there.

Interestingly, after BMP-2 loading, a general increase in cell adhesion and spreading was observed on all BMP-2-loaded PEMs, including the pos Ctrl, indicating a promoting effect of BMP-2 on cell adhesion and spreading. This enhancement was characterized by more spread elongated cells showing more alignment of longitudinal actin filaments (red) and organization of vinculin (green) in FA plaques, as illustrated in the CLSM images (Figure 7E, 2nd and 3rd row). Further, the increase of total length of actin filaments on loaded PEMs was significant for all PEMs compared to nonloaded ones (Figure 7D). Nonetheless, oCS100 PEMs were still superior to oCS50 and nCS PEMs even after loading BMP-2. This was proven not only by showing the longest total actin filaments (Figure 7D) but also by the pronounced organization of the most vinculin in FA (Figure 7C) compared to oCS50 and nCS PEMs.

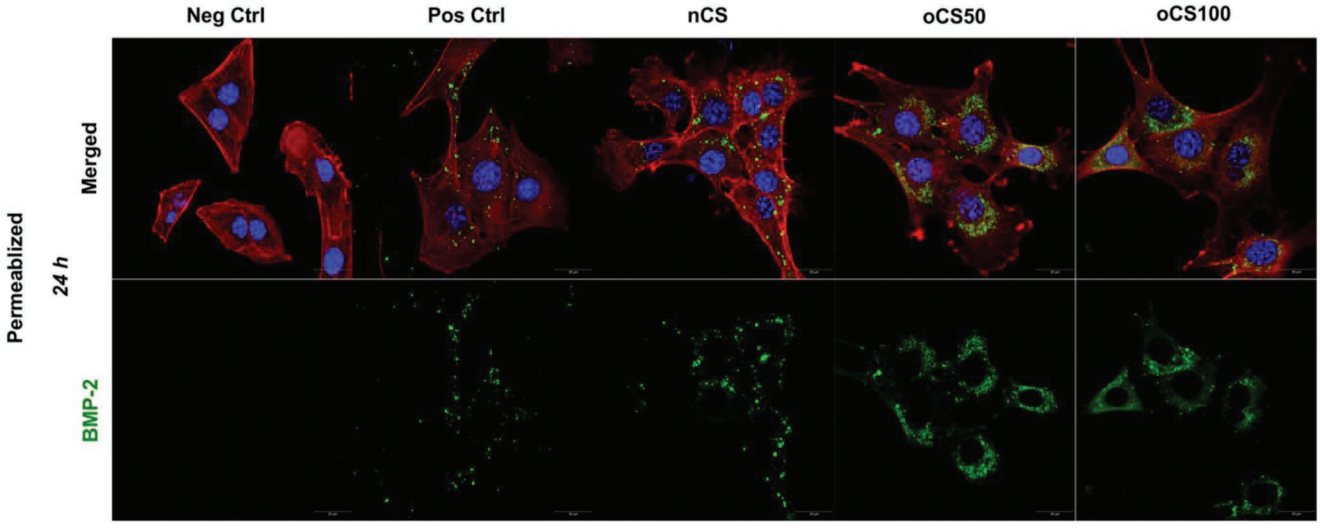

Figure 6. CLSM images show BMP-2 internalization into permeabilized C2C12 cells after 24 h of incubation on BMP-2-loaded PEM. PEMs of oxidized chondroitin sulfate (oCS100), native chondroitin sulfate (nCS), or a mixture of both (oCS50) were prepared with Col I as polycation. The samples were stained for BMP-2 (green) being internalized into the cells, filamentous actin (red), and nucleus (blue). As controls, cells were seeded on plain glass slides either without (neg Ctrl) or with BMP-2 (pos Ctrl) in the medium. Cells were imaged with CLSM 63× oil immersion objective (scale bar: 20 µm).

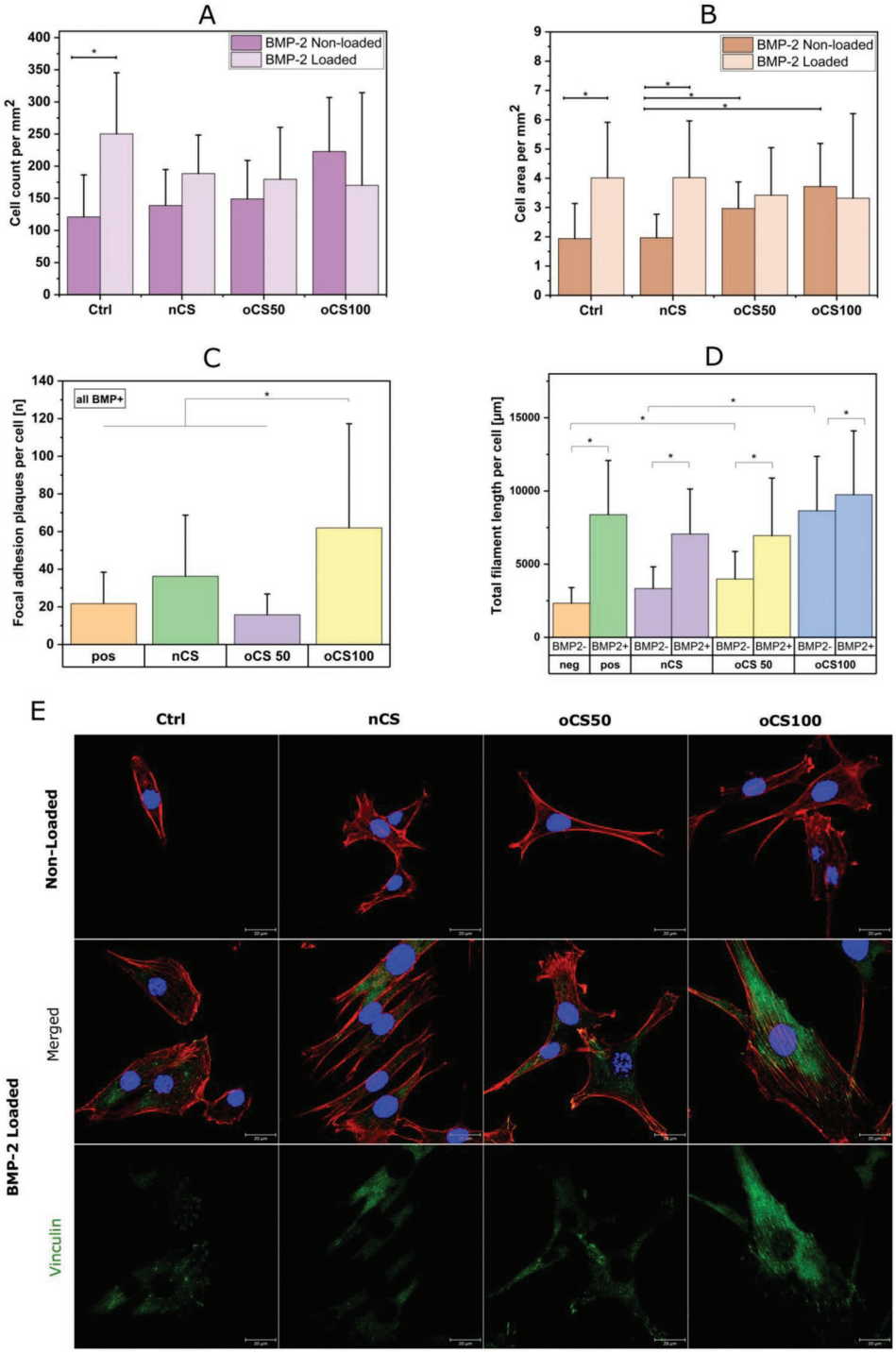

Figure 7. Adhesion of C2C12 cells seeded on native and various cross-linked multilayers, after 24 h of incubation. PEMs of oxidized chondroitin sulfate (oCS100), native chondroitin sulfate (nCS), or a mixture of both (oCS50) were prepared with Col I as polycation. A) Quantification of cell count, B) and cell area obtained using ImageJ. C) Quantification of vinculin in FA plaques. Calculated FA plaques were related to the individual cell area and detected with a custom cell profiler pipeline. $n > 15$, $^*p \leq 0.05$ ANOVA, post-Tukey. D) Actin filament length quantification on both BMP-2-loaded and nonloaded multilayers. All actin fibers were detected by phalloidin. Filament sensor 0.1.7 was used to detect all fibers in each cell. $n > 15$, $^*p \leq 0.05$ ANOVA, post-Tukey. (*) data are significantly different. E) CLSM images show C2C12 cells adhesion after 24 h incubation on various native and cross-linked multilayers. The cells were stained for vinculin (green) present in FAs, filamentous actin (red), and nucleus (blue) on multilayers without BMP-2 (upper row) and with BMP-2 loading (lower row). As a control, cells were seeded on plain glass slides either without (nonloaded) or with BMP-2 (BMP-2 loaded) in the medium. Cells were imaged with CLSM 63× oil immersion objective (scale bar: 20 µm).

2.5. Quantitative and Qualitative Osteogenic Differentiation Studies

To understand whether it is the released BMP-2 or the matrix-bound BMP-2 that is bioactive and able to trigger osteogenesis, quantitative real-time polymerase chain reaction (qRT-PCR) was performed to evaluate the expression of specific osteogenic markers (**Figure 8**). ALP was significantly upregulated in C2C12 cells grown on oCS100 PEMs (≈4.5-fold increase) and oCS50 PEMs (≈3.5-fold increase) compared to the weak increase (≈1.5) in gene expression on nCS PEMs. One exception was for pos Ctrl, where the high concentration (10 µg mL^{-1}) of soluble BMP-2 in the medium triggered very high expression of ALP gene (≈11-fold increase). Further, Col I was also found to be strongly expressed in cells grown on oCS100 PEMs (≈3.5-fold increase) followed by oCS50 PEMs with 2.5-fold increase in Col I gene expression, while reduced expression was measured for cells on nCS PEMs (≈0.5-fold). Interestingly, the soluble BMP-2 in pos Ctrl could not trigger high Col I gene expression. Furthermore, the osteogenic marker Runx2 was upregulated in cells grown on all PEMs in general, with being more pronounced in cells on nCS PEMs and on pos Ctrl with ≈2.5-fold and twofold increase, respectively, and less on oCS100 (≈1.5-fold increase) and oCS50 PEMs (≈1.25-fold increase). Similar finding goes for Osterix which was significantly more upregulated in cells cultured on nCS PEMs and pos Ctrl than on oCS100 and oCS50 PEMs. Noggin which acts as a BMP-2 antagonist[31] was downregulated in cells grown on oCS100 and oCS50 PEMs (≈0.5-fold increase) and upregulated in cells on nCS PEMs and pos Ctrl. It is worth mentioning that a balanced BMP-2/ Noggin level is very important in regulating osteogenesis.[31] The more Noggin is expressed, the less osteogenesis occurs. However, since the expression of genes does not guarantee their translation into proteins,[32] further osteogenic markers on the protein or ECM level were screened.

In **Figure 9**A, it is worth noticing that significantly high ALP activity was observed in cells grown on oCS100 and oCS50 PEMs and not on nCS or pos Ctrl which confirms the PCR data of ALP and Col I expression. These findings were also reflected in the ALP staining and alizarin red staining of the mineralized matrix (Figure 9B) at which the most ALP staining (purple color) was observed for cells on oCS100 and oCS50 PEMs while very little ALP staining (purple) was observed for nCS PEMs and even for pos Ctrl. The same was noted for alizarin red. Big dark red oily spots, representing the mineralized matrix, were observed on oCS100 and oCS50 PEMs compared to the absence of this positive staining on nCS PEMs. Moreover, in the immune staining of Col I and Runx2 (Figure 9C), oCS100 and oCS50 PEMs were also superior to nCS PEMs at which more Col I and Runx2 staining existed on oCS100 and oCS50 PEMs, as visualized in the single channels of Col I (green) and Runx2 (red), while very faint staining is observed on nCS PEMs.

3. Discussion

3.1. Physical Studies on Multilayers Formation and Properties

The multilayers build-up was investigated by QCM-D, which provides information on the total adsorbed mass (containing water) and permits the study of the viscoelastic properties of the multilayers. In all PEMs, more deposition of Col I than of the polyanion was observed, which is probably related to the higher molecular weight of Col I. ΔD increased after addition of Col I followed by a decrease after addition of polyanion, indicating stiffening of PEM after CS adsorption. This is due to the diffusion of CS into the underlying layers of Col I leading to compaction and displacement of water. A similar effect was observed by others for heparin/poly(L-lysine) (PLL) and heparin/chitosan PEMs.[33,34] When an additional Col I layer is adsorbed and the system takes up water, the multilayers swell and become softer again.[35] The PEM assembly was performed at pH 4 at which Col I acquires a net positive charge since its isoelectric point is about 5.5[36] while CS is considered a polyanion with a pK_a value of 2.5.[37] Therefore, our assumption is that the formation of nCS PEMs was mainly depending on ion pairing[38] between positively charged Col I and negatively charged CS whereas in oCS PEMs an additional covalent pairing mechanism was involved, which is the imine bond formation between the aldehyde groups in oCS and the amino groups of Col I.[21] Therefore, in oCS50 PEMs, it is suggested that the polymer binding was mainly depending on the covalent pairing mechanism between oCS and Col I while most of other negatively charged groups on nCS and oCS are remaining free, causing electrostatic repulsion that leads to more swelling and attraction of water. The latter could be the reason behind the higher dissipation and viscoelastic thickness calculated for oCS50 PEMs. This was also proven when comparing the viscoelastic thickness to the dry thickness measured by ellipsometry. Here, oCS50 PEMs had a comparable dry thickness to oCS100 PEMs when water was excluded.

Surface properties of PEMs were studied with WCA and AFM measurements. This is related to the fact that both wetting properties and topography have an effect on cell adhesion and fate.[39] Biophysical cues such as topographical and mechanical features of ECM result in profound effects on cellular morphology and function, through mechanotransduction mechanisms.[40] Cells possess the ability to recognize and respond to the nano- and microscale organization of molecular signals in their ECM.[41] On nanostructured surfaces, cells tend to spread more on the smallest nanostructures accompanied by increased expression of FA while less spreading occurs on macrostructures.[39] Here in our study, the Col I fibers with the various densities and diameters represent both the chemical and topographical cues. The observed moderate wettability of all studied PEMs is favorable for cell adhesion.[42] While CS is known to be highly hydrophilic, Col I is more hydrophobic as a pure film (WCA ~ 110°).[43] Thus, the reason behind these WCA values could be the high mass contribution of Col I in all studied multilayers. A similar WCA was observed by Zhao et al. for CS-based PEMs compared to HA-based PEMs showing lower WCA for the latter due to lesser Col content.[21,22]

Col as ECM molecule plays an important role in cell adhesion, spreading, and differentiation.[44] The soft nature of oCS50 PEMs detected by QCM-D with higher dissipation was confirmed by AFM measurements, which revealed that oCS50 PEMs have the lowest elastic modulus. The intrinsic crosslinking of oCS100 PEMs together with the observed density and

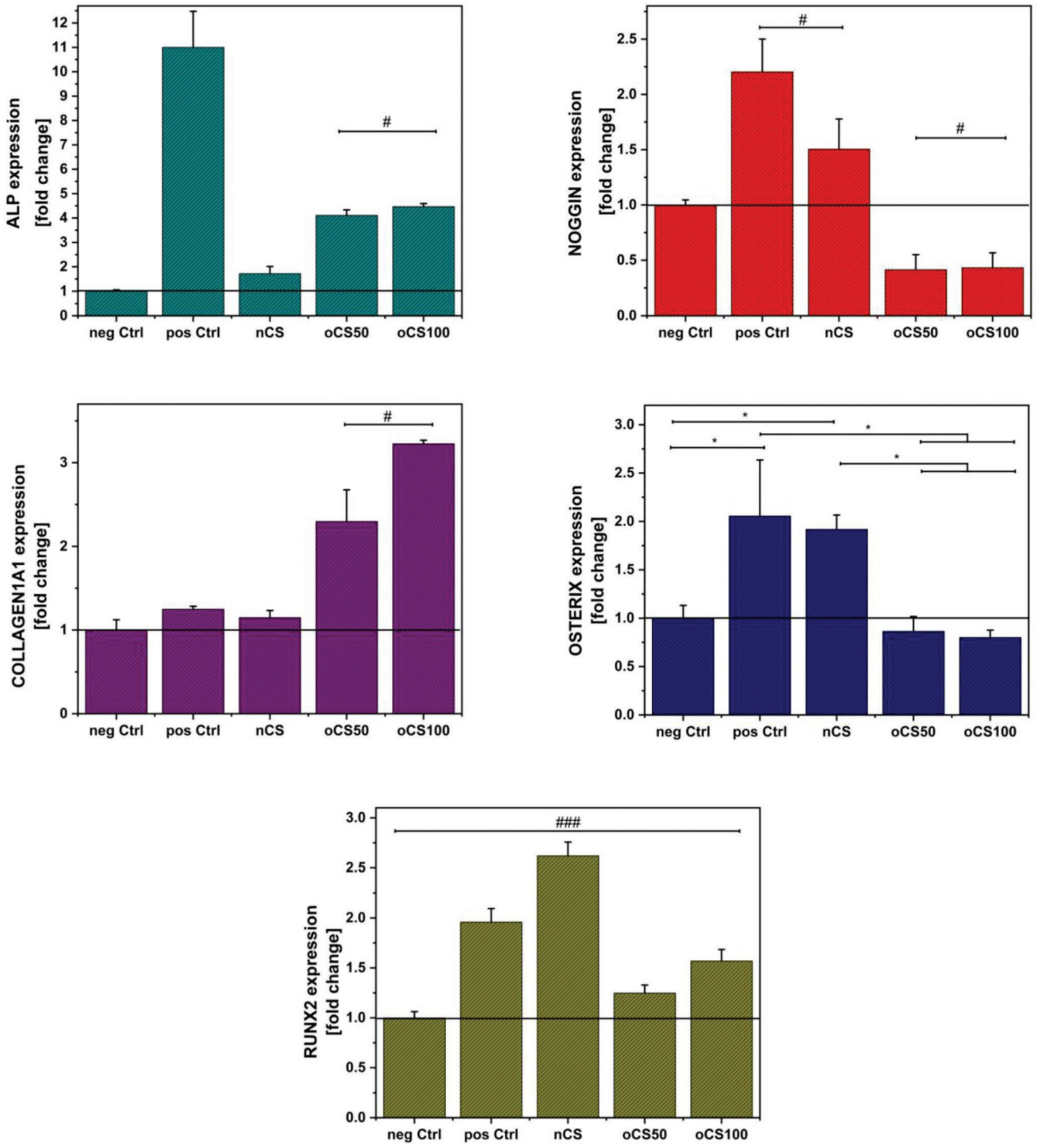

Figure 8. Relative expression of mRNA of osteogenic markers (ALP, Col I, Runx2, Osterix, and Nogging) after 14 days of C2C12 incubation on the various native and cross-linked multilayers. PEMs of oxidized chondroitin sulfate (oCS100), native chondroitin sulfate (nCS), or a mixture of both (oCS50) were prepared with Col I as polycation. qRT-PCR analyses were performed as described in the Experimental Section. Data represent mean ± SD values, $n = 6$, $p \leq 0.05$ and Scheffe post hoc test. (*) data are significantly different. (#) all data are significantly different except. (###) all data are significantly different.

thickness of Col I fibers contributed to its high elastic modulus and roughness compared to nCS PEMs. Further, Col I is self-assembling to form fibrils both in vivo and in vitro.[45] Col I fibrillization results from two successive processes. One is happening during the lag period (nucleation) and the other occurring during the growth phase where nuclei grow into fibrils.[46]

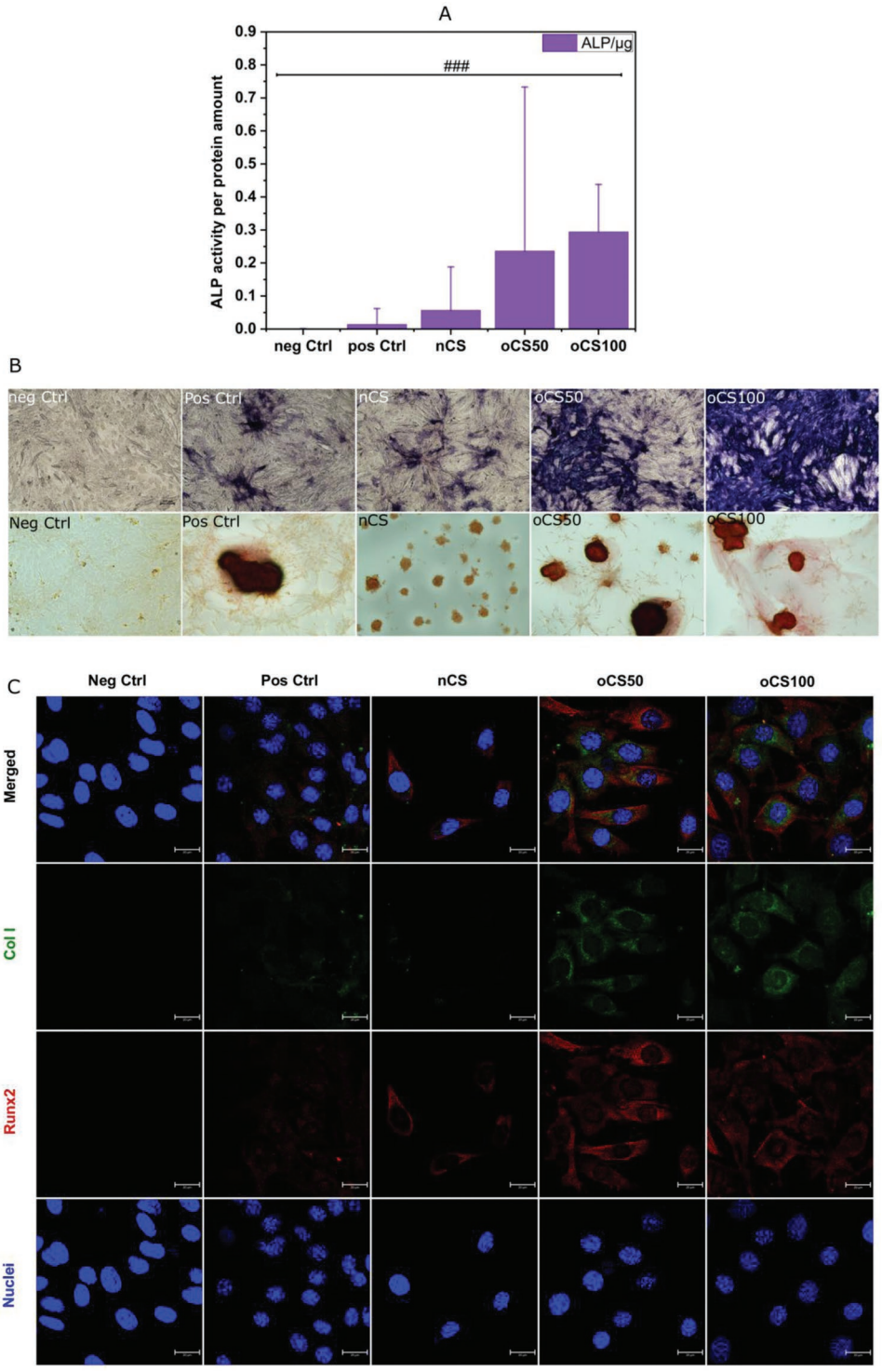

Figure 9. PEMs of oxidized chondroitin sulfate (oCS100), native chondroitin sulfate (nCS), or a mixture of both (oCS50) were prepared with Col I as polycation. A) Measurements of ALP activity in C2C12 cells seeded directly on top of BMP-2-loaded multilayers fabricated in 24-well plate, determined via absorbance measurements at 405 nm after 7 days' incubation time, using a plate reader. Measurements are normalized to the total protein amount (BCA values). **###** indicates that all data are significantly different to each other. B) Bright-field images (10×) of C2C12 cells seeded on various native and cross-linked multilayers and stained after 7 days for ALP, and after 14 days with alizarin red-S solution to investigate the formation of mineralized matrix (scale bar: 100 µm). C) CLSM images show C2C12 cells after 14 days incubation on BMP-2-loaded multilayers. The cells were stained for Col I (green), Runx2 (red), and nucleus (blue). As a control, cells were seeded on plain glass slides either without (neg Ctrl) or with BMP-2 (pos Ctrl) in the medium. Cells were imaged with CLSM 63× oil immersion objective (scale bar: 20 µm).

Col I fibrillogenesis is affected by several factors such as ionic strength, pH, temperature, and the presence of GAGs.[47] It was found that a pH value less than 5.5 enhances the formation of globular Col I structures while a pH value above 5.5 promotes fibrillogenesis.[47,48] However, since the fibrillogenesis occurred in our study even at pH 4, CS seems to play a remarkable role in regulating this process through facilitating the organization of mature Col I fibrils by enhancing Col I concentration.[49] While nCS PEMs rely mainly on ion pairing, it has been suggested that strong electrostatic interaction between the used polyanion and Col I can produce a high number of nucleation sites, which in turn results in a long and retarded lag phase that results in fibers with smaller diameter.[50,51] On the other hand, in oCS50 PEMs, the electrostatic repulsion and steric hindrance resulting from the free charged groups in the mixture of nCS and oCS lead to less induction of nucleation making Col I more available. This higher availability of Col I permits then more lateral aggregation of it and shorter lag phase ending up with fibers of larger diameters.[51,50] Furthermore, the Col I fibrils were prone to either complete or partial dissolution after loading BMP-2, which is due to the acidic pH at which Col I has a net positive charge and is present in a soluble state.[36] However, oCS100 and oCS50 PEMs could save the fibrillar structure of Col I to a certain degree which could be related to the successful crosslinking of Col I in those PEMs. Further, this partial dissolution of Col I fibers led to a decrease in elastic modulus and roughness on all PEMs. One exception was the nCS PEMs, which showed an increase in elastic modulus after BMP-2 loading. We relate this to the function of the AFM cantilever, which interacts with the surface, hence, it could have given a false positive result after the dissolution of Col I fibers and started rather sensing the silicon substrate instead.

3.2. Biological Studies

BMP-2 was expected to be bound to CS in all multilayers via its heparin binding domain, at which positively charged amino acids bind to negatively charged groups on GAGs.[52] Indeed, intrinsic cross-linking of oCS PEMs not only increased sequestering of BMP-2 compared to nCS PEMs as visualized by antibody staining of bound BMP-2, but also resulted in lesser BMP-2 release over time. Since the release of BMP-2 was fitting to the Higuchi model,[30] the release seems to be depending on the cross-linking density related to the mechanism of binding. In nCS PEMs, the multilayers formation (at pH 4) is based on ion pairing[38] and the BMP-2 can be easily entrapped inside the multilayers. When the pH is increased to physiological value (pH 7.4), Col I will be less charged with reduction of ion pairing[38] which leads to faster release of BMP-2. The faster the release is, the more BMP-2 in a soluble state exists (similar to pos Ctrl). Hence, less matrix-bound BMP-2 remains in the multilayers to be presented to the cells, which led to less BMP-2 internalization in cells on nCS PEMs. Further, the imine bonds in oCS PEMs can be partly hydrolyzed at acidic pH permitting uptake of BMP-2 during loading (pH 4) while these bonds are formed and are more stable at neutral and basic pH.[53] Therefore, the loaded BMP-2 is entrapped when the imine bonds are formed. This resulted in the very little release of BMP-2 from oCS100 PEMs and here it is worth pointing out that this very little release indicates that the majority of the loaded BMP-2 is still stored and available to cells in a matrix-bound manner, which is the effective way of GF presentation to the cells that is similar to what happens in the native ECM.[10] The availability of BMP-2 as matrix-bound in oCS100 PEMs allowed its presentation in a spatial/temporal manner to the cells at their ventral side which resulted in more BMP-2 internalization. However, it has been found that BMP-2 signaling can be independent of BMP-2 internalization where signaling can still take place at the plasma membrane even in the absence of BMP-2 internalization.[16,54] Moreover, the swelling and the aqueous nature of oCS50 PEMs indicated previously by AFM and QCM data, resulted in more diffusion of BMP-2 compared to oCS100 PEMs, i.e., more soluble BMP-2. This highlights the strong contribution of the intrinsic cross-linking in oCS100 PEMs in increasing the stability of the multilayers under physiological conditions,[21] and controlling BMP-2 release and presentation.[8]

Cell adhesion is considered as a prerequisite for a variety of cellular function including cell growth and differentiation.[55] C2C12 cells adhered generally on all nonloaded PEMs due to their moderate wettability, observed by WCA that is usually preferred by cells (WCA 40°–70°),[56] and the presence of Col I.[22] Moreover, Col I fibrils are known to promote the adhesion of a variety of cells via integrin-mediated interaction,[57] where $\alpha 2\beta 1$ is the main functioning integrin receptor for Col I fibrils.[58] Thus, on nonloaded PEMs, the thick Col I fibers present on oCS PEMs contributed to significant more cell spreading than on nCS PEMs, as shown by quantification of cell area. In addition, on BMP-2 nonloaded multilayers, cell attachment on control surfaces was the lowest which indicates that there is no intrinsic toxicity of multilayers particularly when using oxidized CS. Necrotic of apoptotic cells have a rather round shape[59] which was not seen there. Furthermore, more elongated cells and more cell spreading characterized by expression of longitudinal actin filaments and vinculin molecules in FA sites were observed on all BMP-2-loaded samples indicating a promoting effect of BMP-2 on cell adhesion.[54] A crosstalk between BMP-2 and integrin-dependent signaling pathways which promotes the formation of FA and stress fibers, was observed in other studies.[54] Additionally, the mechanical properties of the ECM or the substrata are strong modulators of cellular behavior.[60] On stiff surfaces, the cells exert stress by expansion of their FA and increase recruitment of vinculin.[61] This results in an extended and spread shape of cells together with alteration of stress fibers,[62] which goes on well with our findings regarding oCS100 PEMs (both loaded and nonloaded). Vinculin plays a role in strengthening adhesion by increasing the local membrane stiffness, modulating by that bond stressing in the contact area.[63] On the other hand, cell adhesion and spreading are suppressed on soft substrata because of suppressing signaling via integrins regarding mechanotransduction.[35] Since oCS50 PEMs are the softest and most water containing, less vinculin organization was observed compared to oCS100 and even nCS PEMs. Such effect of PEM stiffness on FA and actin organization of C2C12 cells was already shown previously by others using PLL/HA PEM and ethyl-3-(3-dimethylaminopropyl) carbodiimide (EDC) for cross-linking[15] which fits to our findings here. In this study, it was made clear that not only

the topography matters but also the stiffness and the molecular composition together affect the behavior of cells.

The bioactivity of PEMs including the effect of BMP-2 on osteogenic differentiation of C2C12 myoblasts was investigated by qRT-PCR via studying the expression of early osteogenic markers ALP and Col I.[64] These markers were highly upregulated in cells grown on both oCS PEMs compared to the ones on nCS PEMs and pos Ctrl. Ligation of collagen integrin receptors $\alpha 2\beta 1$ and $\beta 1$ integrins in general is required for ALP induction as it increases ALP mRNA triggered by BMP-2.[65] Hence, the presence of thick Col I fibers and the more cell adhesion and spreading could be the reason triggering more osteogenesis in cells grown on oCS100 and oCS50 PEMs compared to nCS PEMs. In addition, the ALP gene expression levels from the qRT-PCR were closely related to ALP staining and activity except for the positive control. The reason for the lack of ALP gene translation could be phosphorylation, proteolysis of core components of the translation machinery, or specific factors such as RNA-binding proteins and miRNA.[32] Moreover, it has been reported that the activity but not the expression of Runx2 is enhanced with osteoblast differentiation in some hMSCs,[66] which could, on one side, explain the reason behind the lower expression of Runx2 in cells grown on oCS PEMs compared to nCS PEMs and pos Ctrl. On the other side, post-transcriptional regulation by miRNAs may affect the expression of Runx2 and Osterix,[67] which could explain the lower level of Osterix expression in cells grown on oCS PEMs compared to nCS. Furthermore, Noggin is a specific antagonist of BMPs that was found to be expressed by osteoblasts to regulate the extracellular exposure to BMP as part of the negative feedback mechanism that prevents the interaction of BMP with its receptor. Therefore, achieving a balance between BMPs and Noggin plays a critical role in regulating osteogenesis.[31] On pos Ctrl and nCS PEMs, cells are exposed to high amounts of soluble BMP-2, triggering by that the expression of osteogenic gene markers together with high Noggin expression. By contrast, matrix-bound BMP-2 presented to cells from oCS PEMs triggered higher expression of osteogenic genes but reduced Noggin. Therefore, this balanced BMP-2/Noggin ratio in oCS PEMs is expected to enable complete osteogenesis in comparison to the unbalanced ratio in pos Ctrl. Osteoblasts start synthesizing their ECM which consists mainly of Col I followed by ALP production and later-stage ECM calcification occurs.[65] Hence, Col I expression and secretion is important for starting and increasing the mineralization process.[66,68] Referring back to the qRT-PCR data, Col I and ALP expression were highly upregulated in cells grown on oCS PEMs while it was almost like the neg Ctrl on nCS PEMs. Thus, more mineralization is expected to occur on oCS PEMs. The latter was proven when looking at Alizarin red staining of the mineralized matrix that was more pronounced in cells cultured on oCS than on nCS PEMs. The findings of qRT-PCR go well with the results detected from CLSM images of immunestaining where more Col I and Runx2 staining were detectable for cells on oCS compared to nCS PEMs and pos Ctrl. Altogether, this confirms that the osteogenic markers expressed in cells grown on oCS PEMs were efficiently translated into proteins and were accompanied with real osteoblast development while this was absent on nCS and pos Ctrl despite offering the soluble BMP-2 in larger amounts.

4. Conclusion and Outlook

The oCS PEMs with intrinsic cross-linking are superior to nCS PEMs in supporting cell adhesion, spreading, and triggering osteogenesis through storage and presentation of the loaded BMP-2 to the cells in a matrix-bound manner rather than releasing it in a soluble state. The intrinsic cross-linking supports the presence of an ECM-like microenvironment through enhancing the stiffness and stability of PEMs and preserving the structure of Col I fibers that represent an ECM-like topographical and chemical cue. The key to achieve the targeted cell differentiation is not only about the quantities of GF released but requires rather a combination between the availability of matrix-bound GF and a slow release profile. Moreover, the moderate releasing profile and the soft nature of oCS50 PEMs could allow their use for articular cartilage regeneration using the growth and differentiation factor-5 (GDF-5) that supports cell differentiation into chondrocytes. Overall, these multilayers with intrinsic cross-linking can be further used as coatings for implants to deliver GFs to the site of defects for bone regeneration application and other tissue defects.

5. Experimental Section

Materials: Cell culture flasks and polystyrene well-plates were purchased from Greiner Bio-one GmbH & Co.KG (Frickenhausen, Germany). Round glass (Ø12 mm) were purchased from VWR (Germany) and glass object holders were provided by Karl Hecht GmbH & Co (Sondheim, Germany). Glutaraldehyde was obtained from AppliChem (Darmstadt, Germany). Collagen I was obtained from Sichuan Mingrang Bio-Tech (Sichuan, China). Chondroitin sulfate (CS), PEI, Triton X-100, and sodium periodate (NaIO4) were provided by Sigma-Aldrich Chemie GmbH (Steinheim, Germany). Trypsin/ethylenediaminetetraacetic acid (EDTA) solution and fetal bovine serum (FBS) were provided by Biochrom (Berlin, Germany). Penicillin/ streptomycin (pen/strep) was from Lonza (Walkersville, MD, USA). Sodium chloride (NaCl), bovine serum albumin (BSA), 4-nitrophenylphosphate disodium salt hexahydrate (*p*-NPP), hydrogen peroxide 35% (H_2O_2), and alizarin red-S were provided by Carl Roth GmbH & Co. KG (Karlsruhe, Germany). Schiff's reagent was from Merck KGaA (Darmstadt, Germany). DMEM (phenol red) and paraformaldehyde 4% (PFA) were provided by Roth (Germany). Dialysis bags (Spectra/Por membrane, M_w cutoff = 3500) were provided by Spectrum Labs (CA, USA). 5-Brom-4-chlor-3-idolylphosphate-*p*-toluidinsalt (BCIP) was purchased from Roth, Germany. While, *p*-Nitro blue tetrazolium chloride (NBT) was purchased from Applichem, Germany. AMP buffer was provided by Roth, Germany. 2-phospho-L-ascorbic acid trisodium salt was from Sigma-Aldrich, Germany and β-glycerol phosphate was from Alfa Aesar, Germany. Mowiol was obtained from Calbiochem (Darmstadt, Germany).

Synthesis of oCS: Native CS (nCS) was used as a polyanion and as a native glycosaminoglycan (nGAG) in all experiments. According to previously published protocol, oxidized CS (oCS) was synthesized.[8] In short, to get 100% theoretical oxidation degree, 1 g of nCS (nCS $M_w \approx 75$ kDa) was dissolved in (200 mL) of ultrapure water and left to react with 0.5 g of $NaIO_4$ for 3 h at room temperature (RT) under stirring and protection from light. Dialysis against distilled water using membrane of 3.5 kDa cut-off was used for 3 days at RT to purify the reacted CS and the final product was obtained by freeze-drying (ALPHA 1–2 LDplus, Christ, Osterode am Harz, Germany) and stored at 4 °C for further use. A photometric detection method known as "Schiff's test" was used, as described previously,[69] to quantify the aldehyde groups present in oCS. Oxidation degree of 2.77% was obtained for oCS.

Preparation of Substrata: Glass coverslips, silicon wafers, polystyrene well plates, and quartz chip Au were used when appropriate as substrate surface in the preparation of PEMs systems. Si wafers (Silicon Materials, Kaufering, Germany) with a size of 10 × 10 mm^2 were used for ellipsometry, while round glass coverslips (ø12 mm) were used as substrata for WCA and cell experiments. Both glass and silicon were cleaned using RCA-1 cleaning method which aimed to removing organic contaminants, thin oxide layer, and ionic contamination.[70] Quartz chip Au purchased from 3T Analytik (Germany) were used for QCM-D studies and were cleaned with 70% ethanol and ultrapure water and dried with a stream of nitrogen before use. Ethanol 70% was used for 15 min to sterile glass before the formation of multilayers.

Preparation of Solutions and Formation of PEMs: The multilayers were built up by dip coating method on the previously mentioned substrata which were selected appropriately depending on the experiment to be done. PEI was dissolved in 0.15 mol L^{-1} sodium chloride (NaCl) solution at a concentration of 2 mg mL^{-1}. Native chondroitin sulfate (nCS), oxidized chondroitin sulfate (oCS100), and oxidized/native chondroitin sulfate mixture (oCS50) were used as polyanions. oCS100 and nCS were dissolved in 0.15 mol L^{-1} NaCl solution at a concentration of 2 mg mL^{-1}. oCS50 solution was obtained by mixing oCS100 and nCS in a 1:1 ratio to get a mixture which contained 50% oCS and 50% nCS. Collagen I (Col I) was used as a polycation and was dissolved at a concentration of 2 mg mL^{-1} in a 0.15 mol L^{-1} NaCl solution containing 0.2 mol L^{-1} acetic acid and stirred at 4 °C overnight followed by centrifugation for 10 min at max speed to eliminate insoluble precipitates. A final working concentration of 0.5 mg mL^{-1} working solution was obtained by diluting the stock solution in 0.15 M sodium chloride and 0.2 mol L^{-1} acetic acid solution.[21] 0.15 mol L^{-1} NaCl was used as a washing solution. All polyelectrolytes were adjusted to pH 4 with exception to PEI with pH 7.4. A 0.2 µm pore size membrane filter (Whatman) was used to filter all polyelectrolytes and washing solution before use.

PEI was used as the first binding layer to obtain a net positive charge and was adsorbed for 30 min on the substrates. Then, for the various systems, alternating layers of polyanions (nCS, oCS100, or oCS50) and polycation (Col I) were used until reaching a total number of 17 layers with Col I being the terminating layer. Polyanions and polycation were alternatively incubated for 15 min followed by 2 × 4 min washing steps using 0.15 mol L^{-1} NaCl solution. All multilayers formation procedures were carried out at RT under gentle shaking (Heidolph, Polymax 1040, at 30 rpm).

Measurement of Multilayers Growth: The layer growth and multilayers formation were investigated via QCM-D monitoring, as previously described.[38] A qCell T temperature-controlled quartz crystal microbalance from 3T analytik (Tuttlingen, Germany) was used for QCM-D measurements. The principle of QCM-D was based on the sensitivity of the quartz sensor to the mass and properties of materials deposited on the surface. During the deposition of materials on the sensor or when an alternating voltage was applied, there was a change in resonant frequency and damping (dissipation). The change in frequency and damping was captured by the device in real-time.[71] Multilayers were built up in the QCM-D flow cell by injecting alternating polyanion/polycation solutions and this was monitored in real-time using quartz chip Au as the substrate surface. The change in frequency and evaluation of layer thickness were carried out using the qCell T device and qGraph software.

WCA Measurements: After the formation of multilayers on glass coverslips, they were stored in a desiccator before carrying out WCA measurements. The wettability properties of multilayer surfaces were determined by static WCA measurements using an OCA15+ device (Dataphysics, Filderstadt, Germany), as previously described.[72] The sessile drop method was implemented using five droplets of 3 µL ultrapure water for each sample. The software of OCA15+ device recorded for each droplet at least ten independent measurements. Measurements were fitted with the ellipse-fitting method and mean and standard deviations for all measurements were calculated.

Characterization of PEMs Dry Thickness: The thickness of PEMs built up on cleaned Si wafers was determined using an M-2000 V scanning ellipsometer (J.A Woollam Co. Inc., Lincoln, NE, USA) with an angle of incidence of 70°. The thickness of formed multilayers was determined by fitting the experimental data to an additional Cauchy layer and a refractive index of 1.36 was used to calculate layer thickness. Finally experimental data obtained were analyzed with the device' software (WVase32).

Measurement of PEMs Surface Topography and Elastic Modulus: Topographical imaging as well as measuring local elasticity of the multilayers (deposited on silicon substrates) was performed using AFM (nanowizard IV, JPK-Instruments, Berlin, Germany) in quantitative imaging mode (QI). Here, a silicon cantilever (FMR, Nanosensors) in a standard liquid cell (JPK-Instruments) containing 0.15 mol L^{-1} NaCl was employed. *JPK Data Processing V5.0.85* and (*Gwyddion V2.49*) software were used for postprocessing, calculation of elasticity, and analyzing roughness parameters. To measure the diameter of the Col I fibers present on the surface, the program *FSegment* was used.[73] While this program was originally developed for actin fiber detection, its line tracing algorithm was also successfully used to detect the Col I fibers found on top of the samples. All settings were kept equal for all samples. The program traced all fibers and measured the width of each fiber every 5 pixel (equals 48.5 nm). All measuring points per sample were then cumulated and analyzed.

Uploading of Recombinant Human Bone Morphogenetic Protein 2 (rhBMP-2) to Multilayers for Cell and Release Studies: After the formation of multilayers, rhBMP-2, produced in a heterologous host of *Escherichia coli* (*E. coli*) according to Hillger et al.,[74] was loaded onto the multilayers. A concentration of 10 µg mL^{-1} rhBMP-2 was used for all experiments and was obtained by diluting the stock solution (50 µg mL^{-1}) with 1 mmol HCl. 200 µL rhBMP-2 was added to each PEM sample and incubated at 4 °C overnight 1 day prior to cell seeding/enzyme-linked immunosorbent assay (ELISA) samples collecting. After incubation, rhBMP-2 was aspirated and layers were washed quickly with 0.15 mol L^{-1} NaCl solution pH 7.4. For positive controls in cell experiments, 10 µg mL^{-1} rhBMP-2 was added directly to the medium and the stock solution was diluted using DMEM cell culture medium instead of 1 mmol HCl.

BMP-2 Release Studies via ELISA: 10 µg mL^{-1} BMP-2 in 1 mmol HCl (50 µL each well) was loaded for overnight at 4 °C to the PEMs which were fabricated in a 96-well plate. Samples were collected over 7 days, each time followed by adding new fresh phosphate-buffered saline (PBS, pH 7.4). An ELISA kit from PeproTech (Hamburg, Germany) was used to check the released amounts of BMP-2. A series of BMP-2 concentrations was used to obtain a standard curve which was used later to calculate the released amounts from the PEMs according to the absorbance values measured at 405 nm.

BMP-2 Staining on Multilayers for Semiquantification: Multilayers were fabricated on glass cover slips and loaded with BMP-2 as mentioned previously. After loading, the samples were incubated in DMEM + 10% FBS (the same medium used for cell experiments) at 37 °C. After 24 h (the first set) and 7 days (the second set), samples were washed with PBS and fixation was done for 15 min using 4% PFA and further 1% BSA was used as a blocking agent with two washing steps with PBS in between. Then, the staining of BMP-2 was done using a primary BMP-2 mouse monoclonal antibody (1:50, Invitrogen) and a secondary CY2-conjugated goat anti-mouse antibody (1:100, Jackson Immuno Research Laboratory, Inc.) for 30 min incubation each, and 3×5 washing times with PBS after each staining step. The samples were then mounted on cover slips with Mowiol (Calbiochem, Darmstadt, Germany) and placed on an object holder. After storage for overnight at 4 °C, samples were visualized with a CLSM (LSM 710, Carl Zeiss, Oberkochen, Germany). The samples were fixed completely flat on the sample holder of the CLSM. Pictures were taken using a 20× objective, open pinhole, and low laser energy to avoid bleaching and gather as much signal as possible. For each measurement, an area of 2125 × 2125 µm was evaluated by using the tiles add-in of Zen 2008 to take a matrix of 5 × 5 individual pictures. The focus was set where the highest mean intensity was reached. Under- and overexposure was avoided carefully. All settings were kept constant during measurements. Finally, the mean intensity of the 8 bit image was extracted by ImageJ 1.53c.

C2C12 (Mouse Myoblast Cell Line) Cell Culture: Cryopreserved C2C12 cells were thawed in a water bath at 37 °C and cultured in DMEM (phenol red) supplied with 10% FBS and 1% penicillin/streptomycin (pen/strep) in a F75 culture flask and incubated in a humidified 5% CO_2/95% air atmosphere in a NUAIRE DH autoflow air-jacketed incubator (NuAire Corp., Plymouth, USA). When cells were about 80% confluence, cells were washed with PBS pH 7.4 and detached from the flask using 0.25% trypsin/EDTA for 3 min at 37 °C, then trypsin action was blocked using DMEM medium containing 10% FBS + 1% pen/strep. Cells were collected in a 15 mL falcon tube and centrifuged at 250 *g* for 5 min, the supernatant was collected and pellet was re-suspended in 1 mL (DMEM + 10% FBS + 1% pen/strep). A 1:100 dilution was made and cells were counted using the Neubauer counting chamber and seeded as needed.

C2C12 Cell Adhesion Studies: C2C12 cells were seeded on the various PEM made on glass cover slips and loaded with BMP-2 as mentioned previously. Two sets of samples were used here; BMP-2-loaded ones and non-BMP-2-loaded ones using positive and negative controls samples as defined above. The density of C2C12 used for each samples was 50 000 cells mL^{-1} in DMEM medium supplemented with 10% FBS. After incubating for 24 h at 37 °C, the same fixation, permeabilization, and blocking steps mentioned above, were employed. For the immune staining, cells were stained with ToPro3 (1:500, Invitrogen) for nucleus, Bodipy-Phalloidin (1:50, Invitrogen) for actin filaments and a primary mouse antibody against vinculin (1:50, Santa Cruz Biotechnology) which was followed by incubation with a CY2-conjugated goat anti-mouse antibody (1:100, Jackson Immuno research Laboratory, Inc.). Samples were incubated with each staining agent/antibody for 30 min in the dark at RT. After each staining step, 3 × 5 min rinsing steps with PBS were performed. Samples were mounted on cover slips with Mowiol as described before. Images were visualized using CLSM with 10x, 20x, and 63x oil immersion objective lenses. Images were analyzed with ZEN 2011 software (Carl Zeiss) and later with ImageJ (1.53c) for cell count and area. For actin length quantification, at least 15 pictures per condition were taken. Contrast of pictures was enhanced with the "Enhance Contrast" function of ImageJ 1.53c. Additionally, all cells touching the image borders as well as dead cell fragments were removed from each picture manually with ImageJ. Afterward, the program filament sensor 0.1.7 developed by Eltzner et al.[75] was used to detect the actin fibers automatically. The settings were kept the same for all samples of the experiment.

The detection of FA was carried out with a custom cell profiler pipeline using Cell Profiler 2.2. The individual cells were segmented with the help of TwoPro3 staining, which was associated with the nuclei and phalloidin staining, which was used to quantify the cytoplasm area. This was done by an automatic thresholding of both areas, a subsequent deduction of the nucleus area from the cytoplasm area, and a parent–child association of the cytoplasm of each cell. FA plaques were made visible by a primary vinculin antibody and subsequent cy2 secondary antibody. To increase the contrast, an enhance feature texture function was used and the FA plaques were detected by thresholding in the individual cell cytoplasm areas. All settings were kept constant over all samples.

BMP-2 Internalization: Multilayers were fabricated on glass cover slips and loaded with BMP-2 as mentioned previously. After overnight incubation, BMP-2 was aspirated and PEMs were washed quickly with NaCl pH 7.4. C2C12 cells were seeded on the various multilayers at a density of 50 000 cells mL^{-1} in (DMEM + 10% FBS) for 24 h at 37 °C. Positive and negative controls were cells seeded directly on glass, with adding the 10 µg mL^{-1} BMP-2 directly to the medium and without adding any BMP-2, respectively. After 24 h, the medium was removed and cells were washed quickly with PBS followed by a fixation step using PFA 4% for 15 min. After that, the samples were divided into two sets: permeabilized and nonpermeabilized. The cell permeabilization was performed using 0.1% triton for 10 min. Thereafter, 1% BSA solution was used as blocking agent for both sets of samples for 1 h. Two washing times using PBS were employed after each step. Afterward, incubation with each antibody for 30 min took place, starting with a primary BMP-2 mouse monoclonal antibody (1:50, Invitrogen), a secondary CY2-conjugated goat anti-mouse antibody (1:100, Jackson Immuno Research Laboratory, Inc.), Bodipy-Phalloidin (1:50, Invitrogen) for actin filaments and ToPro3 (1:1000, Invitrogen) for the nucleus staining. 3×5 washing times with PBS after each incubation step was performed. Stained samples were mounted on cover slips with Mowiol and placed on an object holder and stored at 4 °C for the next day. Using a CLSM, samples were visualized with 63x oil immersion objective lens. Images were processed with the ZEN 2011 software (Carl Zeiss).

Osteogenic Cell Differentiation Studies: ALP Assay: C2C12 cells were seeded at a density of 50 000 cells mL^{-1} in (DMEM + 10% FBS + 1% Pen/strep) on PEMs fabricated directly in a 24-well plate and loaded with BMP-2 as mentioned before. Positive/negative controls were cells seeded directly on well plate with and without BMP-2 addition, respectively, as mentioned previously. After 7 days of incubation, cells were washed with PBS and cell lysis was performed using 1% Triton X-100 for 30 min under slow shaking. Afterward, 1 mg mL^{-1} *p*-NPP was incubated with 50 µL of cell lysate in a 96-well plate for 30 min at 37 °C and the absorbance was measured using a plate reader (FLUOstar OPTIMA, BMG LABTECH) at 405 nm wavelength. The alkaline phosphatase values were normalized to the total protein content that was measured using a Pierce BCA Protein Assay Kit from Thermo scientific (Rockford, IL, USA).

ALP Staining: The same cell seeding procedure used for ALP assay was used here. After 7 days of incubation, cells were washed with PBS and fixed using 2.5% glutaraldehyde solution for 10 min followed by a washing step with AMP buffer. ALP staining mixture included: 25 mg mL^{-1} NBT and 25 mg mL^{-1} BCIP that were prepared in 70% and 100% dimethylformamide, respectively. For every 5 mL AMP buffer, 33 µL NBT and 16 µL BCIP were added to form the ALP staining reagents mixture. After fixation, cells were incubated with the staining reagents mixture in the dark for 1 h at RT. The reaction was then stopped with 20×10^{-3} M EDTA and images were taken using a bright-field NIKON microscope 10x lens and analyzed using NIS element imaging software version 5.10.00.

Alizarin Red Staining: Alizarin red staining was done to determine the deposition of mineralized matrix after 14 days following the same cell seeding procedure and BMP-2 loading, on PEMs made on glass. 1 g of alizarin red was dissolved in 50 mL ultrapure water and pH was adjusted to 4.1–4.3 with 0.5% NH3 and filtered before use. Cells were rinsed once with PBS and fixed with 4% PFA for 15 min then rinsed twice with water. 1 mL of alizarin red was used to stain the fixed cells and incubated in the dark for 45 min at RT. After the incubation period, the stained cells were rinsed twice with ultrapure water and 1 mL PBS was added. Bright-field mages were taken using NIKON microscope with 10x lens and analyzed with NIS element imaging software version 5.10.00.

Immune Staining for Osteogenic Differentiation: PEMs made on glass were loaded with BMP-2 and C2C12 cells were seeded, fixed, permeabilized, blocked, and immune-stained as mentioned in the cell adhesion studies paragraph. For osteogenic differentiation, cells were incubated for 14 days and were stained with ToPro3 for the nucleus, a primary mouse antibody against collagen I (Col I A2) (1:50, Santa Cruz) followed by a CY2-conjugated goat anti-mouse antibody (1:100, Jackson Immuno research Laboratory, Inc.) and a primary rabbit antibody against Runx-related transcription factor 2 (Runx2) (1:50, Biorbyt) followed by a CY3-conjugated goat anti-rabbit antibody (1:100, Jackson Immuno research Laboratory, Inc.). Images were visualized using CLSM with 63x oil immersion objective lens and later were analyzed with ZEN 2011 software (Carl Zeiss).

Extraction of RNA and qRT-PCR: C2C12 cells were seeded at a density of 50 000 cell mL^{-1}) on the various multilayers surfaces that were fabricated in a 24-well plate. After incubation of cells in DMEM medium supplemented with 2% FBS and 1% Pen/Strep for 14 days, RNA was extracted from the cultured C2C12 cells according to the manufacturer's protocol using the Aurum Total RNA Mini Kit from BioRad (Hercules, CA, USA). The first strand of cDNA was synthesized in 20 µL reactions using an iScript Advanced cDNA Synthesis Kit for RT-qPCR according to manufacturer's procedure (Biorad, Hercules, CA, USA). Quantitative Real-Time PCR was carried out under standard enzyme and cycling state on a CFX Connect Real-Time PCR Detection system (Biorad, Hercules, CA, USA). Primer sets were confirmed by PrimePCR Probe Assays for the transcription factors (ALP, COL1A1, Runx2, SP7, and Nog), mentioned in **Table 1**. RPLP0 housekeeping gene was used in this analysis. Data were

Table 1. Primers of osteogenic transcription factors and housekeeping gene used for qRT-PCR.

Symbol	Transcription factor/Name	Assay ID
ALP	Alkaline phosphatase	qMmuCIP0028321
COL1A1	Collagen type 1 alpha 1	qMmuCEP0052648
Runx2	Run-related transcription factor 2	qMmuCEP0057696
SP7	Osterix	qMmuCEP0042201
Nog	Noggin	qMmuCEP0058332
Housekeeping gene RPLP0	60S acidic ribosomal protein P0	qMmuCEP0042968

analyzed using the BioRad CFX Manager Software 3.0 (Hercules, CA, USA). qRT-PCR was carried out under the following conditions: 95 °C for 30 s, then 39 cycles at 95 °C for 15 s and 60 °C for 30 s. The relative gene expression levels were calculated and normalized to the housekeeping gene RPLP0 by the DDCt method ($2-\Delta\Delta Ct$).

Statistics: Statistical calculations were carried out with Origin 8 software. Mean, standard deviation, analysis of significance (analysis of variance (ANOVA)), Kruskal–Wallis, and Dunn post hoc were calculated and described in the respective figures. A value of $p \leq 0.05$ was considered to be significantly different and was indicated by (*). On the other hand, (#) was used to indicate that all data were significantly different except the indicated ones. (###) meant that all data were significantly different to each other. Further, box-whisker diagrams were shown where appropriate. The box indicated the 25th and 75th percentiles, the median (line), and the mean value (square).

Supporting Information

Supporting Information is available from the Wiley Online Library or from the author.

Acknowledgements

The authors are very thankful to Prof. Elisabeth Schwarz for the delivery of BMP-2 that was used in this study. This work was done in the frame of the International Graduate School AGRIPOLY supported by the European Regional Development Fund (ERDF) and the Federal State Saxony-Anhalt. This work was further supported by Fraunhofer Internal Programs under grant no. Attract 069–608203 (C.E.H.S.).

Conflict of Interest

The authors declare no conflict of interest.

Data Availability Statement

The data that support the findings of this study are available in the supplementary material of this article.

Keywords

collagen, glycosaminoglycans, growth factor delivery, intrinsic cross-linking, layer-by-layer technique, osteogenic differentiation

Received: July 21, 2022
Revised: November 10, 2022
Published online: January 23, 2023

[1] A. Mansour, M. A. Mezour, Z. Badran, F. Tamimi, *Tissue Eng., Part A* **2017**, *23*, 1436.
[2] A. Khojasteh, H. Behnia, N. Naghdi, M. Esmaeelinejad, Z. Alikhassy, M. Stevens, *Oral Surg., Oral Med., Oral Pathol. Oral Radiol.* **2013**, *116*, e405.
[3] B. D. Ratner, A. S. Hoffman, F. J. Schoen, J. E. Lemons, *MRS Bull.* **2006**, *31*, 59.
[4] R. O. Hynes, *Science* **2009**, *326*, 1216.
[5] C. Frantz, K. M. Stewart, V. M. Weaver, *J. Cell Sci.* **2010**, *123*, 4195.
[6] A. D. Theocharis, S. S. Skandalis, C. Gialeli, N. K. Karamanos, *Adv. Drug Delivery Rev.* **2016**, *97*, 4.
[7] A. Köwitsch, G. Zhou, T. Groth, *J. Tissue Eng. Regener. Med.* **2018**, *12*, e23.
[8] R. Anouz, A. Repanas, E. Schwarz, T. Groth, *Macromol. Biosci.* **2018**, *18*, 1800283.
[9] T. Katagiri, A. Yamaguchi, M. Komaki, E. Abe, N. Takahashi, T. Ikeda, V. Rosen, J. M. Wozney, A. Fujisawa-Sehara, T. Suda, *J. Cell Biol.* **1994**, *127*, 1755.
[10] R. Anouz, T. Groth, in *Soft Matter for Biomedical Applications* (Eds: H. S. Azevedo, J. F. Mano, J. Borges), Royal Society of Chemistry, London **2021**, pp. 326.
[11] M. S. Niepel, D. Peschel, X. Sisquella, J. A. Planell, T. Groth, *Biomaterials* **2009**, *30*, 4939.
[12] K. Kirchhof, A. Andar, H. Yin, N. Gadegaard, M. Riehle, T. Groth, *Lab Chip* **2011**, *11*, 3326.
[13] J. Borges, J. F. Mano, *Chem. Rev.* **2014**, *114*, 8883.
[14] C. Monge, J. Almodóvar, T. Boudou, C. Picart, *Adv. Healthcare Mater.* **2015**, *4*, 811.
[15] K. Ren, T. Crouzier, C. Roy, C. Picart, *Adv. Funct. Mater.* **2008**, *18*, 1378.
[16] F. Gilde, L. Fourel, R. Guillot, I. Pignot-Paintrand, T. Okada, V. Fitzpatrick, T. Boudou, C. Albiges-Rizo, C. Picart, *Acta Biomater.* **2016**, *46*, 55.
[17] G. Apte, A. Repanas, C. Willems, A. Mujtaba, C. E. Schmelzer, A. Raichur, F. Syrowatka, T. Groth, *Macromol. Biosci.* **2019**, *19*, 1900181.
[18] G. V. Martins, E. G. Merino, J. F. Mano, N. M. Alves, *Macromol. Biosci.* **2010**, *10*, 1444.
[19] S. Ber, G. T. Köse, V. Hasırcı, *Biomaterials* **2005**, *26*, 1977.
[20] Y. Yang, A. Köwitsch, N. Ma, K. Mäder, I. Pashkuleva, R. L. Reis, T. Groth, *J. Bioact. Compat. Polym.* **2016**, *31*, 191.
[21] M. Zhao, L. Li, C. Zhou, F. Heyroth, B. Fuhrmann, K. Maeder, T. Groth, *Biomacromolecules* **2014**, *15*, 4272.
[22] M. Zhao, G. Altankov, U. Grabiec, M. Bennett, M. Salmeron-Sanchez, F. Dehghani, T. Groth, *Acta Biomater.* **2016**, *41*, 86.
[23] A. D. Theocharis, D. Manou, N. K. Karamanos, *FEBS J.* **2019**, *286*, 2830.
[24] J. Bonor, E. L. Adams, B. Bragdon, O. Moseychuk, K. J. Czymmek, A. Nohe, *J. Cell. Physiol.* **2012**, *227*, 2880.
[25] T. Crouzier, K. Ren, C. Nicolas, C. Roy, C. Picart, *Small* **2009**, *5*, 598.
[26] J. A. Phillippi, E. Miller, L. Weiss, J. Huard, A. Waggoner, P. Campbell, *Stem Cells* **2008**, *26*, 127.
[27] N. M. Alves, C. Picart, J. F. Mano, *Macromol. Biosci.* **2009**, *9*, 776.
[28] A. Weltrowski, M. L. da Silva Almeida, D. Peschel, K. Zhang, S. Fischer, T. Groth, *Macromol. Biosci.* **2012**, *12*, 740.
[29] T. Crouzier, L. Fourel, T. Boudou, C. Albigès-Rizo, C. Picart, *Adv. Mater.* **2011**, *23*, H111.
[30] S. Dash, P. N. Murthy, L. Nath, P. Chowdhury, *Acta Pol. Pharm.* **2010**, *67*, 217.
[31] J. Fan, H. Park, S. Tan, M. Lee, *PLoS One* **2013**, *8*, e72474.
[32] R. de Sousa Abreu, L. O. Penalva, E. M. Marcotte, C. Vogel, *Mol. BioSyst.* **2009**, *5*, 1512.
[33] T. Crouzier, C. Picart, *Biomacromolecules* **2009**, *10*, 433.

[34] M. Lundin, F. Solaqa, E. Thormann, L. Macakova, E. Blomberg, *Langmuir* **2011**, *27*, 7537.
[35] N. Aggarwal, N. Altgärde, S. Svedhem, G. Michanetzis, Y. Missirlis, T. Groth, *Macromol. Biosci.* **2013**, *13*, 1327.
[36] N. Barbani, L. Lazzeri, C. Cristallini, M. G. Cascone, G. Polacco, G. Pizzirani, *J. Appl. Polym. Sci.* **1999**, *72*, 971.
[37] K. E. Kuettner, A. Lindenbaum, *Biochim. Biophys. Acta* **1965**, *101*, 223.
[38] N. Aggarwal, N. Altgärde, S. Svedhem, K. Zhang, S. Fischer, T. Groth, *Langmuir* **2013**, *29*, 13853.
[39] B. K. Ekambaram, M. S. Niepel, B. Fuhrmann, G. Schmidt, T. Groth, *ACS Biomater. Sci. Eng.* **2018**, *4*, 1820.
[40] a) G. Chu, Z. Yuan, C. Zhu, P. Zhou, H. Wang, W. Zhang, Y. Cai, X. Zhu, H. Yang, B. Li, *Acta Biomater.* **2019**, *92*, 254; b) M. Aragona, T. Panciera, A. Manfrin, S. Giulitti, F. Michielin, N. Elvassore, S. Dupont, S. Piccolo, *Cell* **2013**, *154*, 1047; c) Y. Xia, X. Fan, H. Yang, L. Li, C. He, C. Cheng, R. Haag, *Small* **2020**, *16*, 2003010.
[41] N. M. Alves, I. Pashkuleva, R. L. Reis, J. F. Mano, *Small* **2010**, *6*, 2208.
[42] J. H. Lee, G. Khang, J. W. Lee, H. B. Lee, *J. Colloid Interface Sci.* **1998**, *205*, 323.
[43] F. Taraballi, S. Zanini, C. Lupo, S. Panseri, C. Cunha, C. Riccardi, M. Marcacci, M. Campione, L. Cipolla, *J. Colloid Interface Sci.* **2013**, *394*, 590.
[44] E. Gurdak, P. G. Rouxhet, C. C. Dupont-Gillain, *Colloids Surf., B* **2006**, *52*, 76.
[45] Z. Keresztes, P. Rouxhet, C. Remacle, C. Dupont-Gillain, *J. Biomed. Mater Res., Part A* **2006**, *76*, 223.
[46] G. Wood, *Biochem. J.* **1960**, *75*, 605.
[47] M. Raspanti, M. Viola, M. Sonaggere, M. E. Tira, R. Tenni, *Biomacromolecules* **2007**, *8*, 2087.
[48] F. Gobeaux, G. Mosser, A. Anglo, P. Panine, P. Davidson, M.-M. Giraud-Guille, E. Belamie, *J. Mol. Biol.* **2008**, *376*, 1509.
[49] A. J. Kvist, A. E. Johnson, M. Mörgelin, E. Gustafsson, E. Bengtsson, K. Lindblom, A. Aszodi, R. Fässler, T. Sasaki, R. Timpl, *J. Biol. Chem.* **2006**, *281*, 33127.
[50] D. Stamov, M. Grimmer, K. Salchert, T. Pompe, C. Werner, *Biomaterials* **2008**, *29*, 1.
[51] D. A. Parry, M. H. Flint, G. C. Gillard, A. S. Craig, *FEBS Lett.* **1982**, *149*, 1.
[52] E. M. Munoz, R. J. Linhardt, *Arterioscler., Thromb., Vasc. Biol.* **2004**, *24*, 1549.
[53] Y. Tao, S. Liu, Y. Zhang, Z. Chi, J. Xu, *Polym. Chem.* **2018**, *9*, 878.
[54] E. Migliorini, A. Valat, C. Picart, E. A. Cavalcanti-Adam, *Cytokine Growth Factor Rev.* **2016**, *27*, 43.
[55] T. Groth, Z.-M. Liu, M. Niepel, D. Peschel, K. Kirchhof, G. Altankov, N. Faucheux, in *Advances in Regenerative Medicine: Role of Nanotechnology, and Engineering Principles* (Eds: V. P. Shastri, G. Altankov, A. Lendlein), Springer, New York **2010**, pp. 253–284.
[56] Y. Arima, H. Iwata, *Biomaterials* **2007**, *28*, 3074.
[57] N. M. Coelho, C. González-García, J. Planell, M. Salmerón-Sánchez, G. Altankov, *Eur. Cells Mater.* **2010**, *19*, 262.
[58] J. Jokinen, E. Dadu, P. Nykvist, J. Käpylä, D. J. White, J. Ivaska, P. Vehviläinen, H. Reunanen, H. Larjava, L. Häkkinen, *J. Biol. Chem.* **2004**, *279*, 31956.
[59] W. Lieberthal, V. Triaca, J. Levine, *Am. J. Physiol.: Renal Physiol.* **1996**, *270*, F700.
[60] M. S. Niepel, B. K. Ekambaram, C. E. Schmelzer, T. Groth, *Nanoscale* **2019**, *11*, 2878.
[61] W. H. Ziegler, R. C. Liddington, D. R. Critchley, *Trends Cell Biol.* **2006**, *16*, 453.
[62] J. Blacklock, A. Vetter, A. Lankenau, D. Oupický, H. Möhwald, *Biomaterials* **2010**, *31*, 7167.
[63] D. W. Dumbauld, H. Shin, N. D. Gallant, K. E. Michael, H. Radhakrishna, A. J. García, *J. Cell. Physiol.* **2010**, *223*, 746.
[64] P. J. Marie, O. Fromigué, *Regener. Med.* **2006**, *1*, 539.
[65] A. Jikko, S. E. Harris, D. Chen, D. L. Mendrick, C. H. Damsky, *J. Bone Miner. Res.* **1999**, *14*, 1075.
[66] R. Marom, I. Shur, R. Solomon, D. Benayahu, *J. Cell. Physiol.* **2005**, *202*, 41.
[67] M. T. Valenti, L. Dalle Carbonare, M. Mottes, *Int. J. Mol. Sci.* **2017**, *18*, 41.
[68] A. M. Ferreira, P. Gentile, V. Chiono, G. Ciardelli, *Acta Biomater.* **2012**, *8*, 3191.
[69] M. Muhammad, C. Willems, J. Rodríguez-Fernández, G. Gallego-Ferrer, T. Groth, *Biomolecules* **2020**, *10*, 1185.
[70] W. Kern, *J. Electrochem. Soc.* **1990**, *137*, 1887.
[71] D. Kömpf, J. Held, S. F. Müller, H. R. Drechsel, S. C. Tschan, H. Northoff, B. Mordmüller, F. K. Gehring, *Malar. J.* **2016**, *15*, 317.
[72] A. Köwitsch, Y. Yang, N. Ma, J. Kuntsche, K. Mäder, T. Groth, *Biotechnol. Appl. Biochem.* **2011**, *58*, 376.
[73] H. Rogge, N. Artelt, N. Endlich, K. Endlich, *J. Microsc.* **2017**, *268*, 129.
[74] F. Hillger, G. Herr, R. Rudolph, E. Schwarz, *J. Biol. Chem.* **2005**, *280*, 14974.
[75] B. Eltzner, C. Wollnik, C. Gottschlich, S. Huckemann, F. Rehfeldt, *PLoS One* **2015**, *10*, e0126346.